Nanoscale

ROYAL SOCIETY OF CHEMISTRY

PAPER

View Article Online
View Journal | View Issue

Cite this: *Nanoscale*, 2023, **15**, 19268

Water-soluble ionic carbon nitride as unconventional stabilizer for highly catalytically active ultrafine gold nanoparticles†

Mohamed M. Elnagar, ‡[a] Johannes Liessem,‡[a] Changbin Im,‡[a] Dariusz Mitoraj, [a] Ludwig A. Kibler, [a] Christof Neumann, [b] Andrey Turchanin, [b] Robert Leiter,[c] Ute Kaiser,[c] Timo Jacob, *[a,d,e] Igor Krivtsov *[a,f] and Radim Beranek *[a]

Ultrafine metal nanoparticles (NPs) hold promise for applications in many fields, including catalysis. However, ultrasmall NPs are typically prone to aggregation, which often leads to performance losses, such as severe deactivation in catalysis. Conventional stabilization strategies (*e.g.*, immobilization, embedding, or surface modification by capping agents) are typically only partly effective and often lead to loss of catalytic activity. Herein, a novel type of stabilizers based on water-soluble ionic (K^+ and Na^+ containing) polymeric carbon nitride (*i.e.*, K,Na-poly(heptazine imide) = K,Na-PHI) is reported that enables effective stabilization of highly catalytically active ultrafine (size of ~2–3 nm) gold NPs. Experimental and theoretical comparative studies using different structural units of K,Na-PHI (*i.e.*, cyanurate, melonate, cyamelurate) indicate that the presence of functionalized heptazine moieties is crucial for the synthesis and stabilization of small Au NPs. The K,Na-PHI-stabilized Au NPs exhibit remarkable dispersibility and outstanding stability even in solutions of high ionic strength, which is ascribed to more effective charge delocalization in the large heptazine units, resulting in more effective electrostatic stabilization of Au NPs. The outstanding catalytic performance of Au NPs stabilized by K,Na-PHI is demonstrated using the selective reduction of 4-nitrophenol to 4-aminophenol by $NaBH_4$ as a model reaction, in which they outperform even the benchmark "naked" Au NPs electrostatically stabilized by excess $NaBH_4$. This work thus establishes ionic carbon nitrides (PHI) as alternative capping agents enabling effective stabilization without compromising surface catalysis, and opens up a route for further developments in utilizing PHI-based stabilizers for the synthesis of high-performance nanocatalysts.

Received 11th July 2023,
Accepted 13th November 2023

DOI: 10.1039/d3nr03375a

rsc.li/nanoscale

Introduction

Ultrafine and highly dispersed metal nanoparticles (NPs) exhibit unique optical, electronic and surface properties, and hold promise for application in various fields, including nanotechnology, optoelectronics, biomedicine, sensing, and catalysis.[1–12] In the field of heterogeneous catalysis, ultrafine (*i.e.*, particles with an average size of *ca.* ≤3 nm) metal NPs often show enhanced catalytic properties that are distinct from their larger counterparts due to the effects of electron energy quantization and surface geometry, *i.e.*, specific surface atom arrangement and coordination.[13,14] For example, ultrafine gold NPs, owing to their large surface area, exposing various surface facets, and a high number of undercoordinated atoms at edge and corner sites, are known to exhibit extraordinary performance in various catalytic conversions, such as CO oxidation, hydrogenation, oxidation of alcohols, coupling reactions, and reduction reactions.[15–19] However, ultrafine metal NPs are thermodynamically and kinetically unstable and tend to aggregate in order to reduce the surface free energy, often resulting in a drastic loss of catalytic performance over time, and thus limiting their practical application.[20,21] Typical strategies to stabilize NPs consist in immobilization on high surface area

[a]*Institute of Electrochemistry, Ulm University, Albert-Einstein-Allee 47, 89081 Ulm, Germany. E-mail: radim.beranek@uni-ulm.de, timo.jacob@uni-ulm.de, krivtsovigor@uniovi.es*
[b]*Institute of Physical Chemistry, Jena Center for Soft Matter (JCSM) and Center for Energy and Environmental Chemistry Jena (CEEC), Friedrich Schiller University Jena, Lessingstr. 10, 07743 Jena, Germany*
[c]*Electron Microscopy of Materials Science, Central Facility for Electron Microscopy, Ulm University, Albert-Einstein-Allee 11, 89081 Ulm, Germany*
[d]*Helmholtz-Institute-Ulm (HIU) Electrochemical Energy Storage, Helmholtzstr. 11, 89081 Ulm, Germany*
[e]*Karlsruhe Institute of Technology (KIT), P.O. Box 3640, 76021 Karlsruhe, Germany*
[f]*Department of Chemical and Environmental Engineering, University of Oviedo, 33006 Oviedo, Spain*

†Electronic supplementary information (ESI) available. See DOI: https://doi.org/10.1039/d3nr03375a

‡These authors contributed equally to this work.

supports, embedding into molecular cage-like materials (*e.g.*, metal–organic frameworks, MOFs), or surface protection by molecules or ions that can act as effective capping agents.[2,22–32] However, all these strategies have also drawbacks. The supported catalysts often exhibit decreased activity as compared to colloidal NPs,[33] and suffer from nanoparticle migration and aggregation, irregular distribution and regrowth, and weak affinity of metal NPs to supports, resulting in increased leaching.[2] The applicability of MOF-embedded metal NPs in catalysis is often limited due to MOF stability issues under catalytic conditions.[34] Finally, the surface capping agents can not only inhibit aggregation but also block the active sites on the NP surface, leading to reduced catalytic activities.[22,23,35] A typical example would be the strongly inhibiting effect of low-weight thiolated polyethylene glycol (HS-PEG) as a stabilizing ligand on the catalytic activity of Au NPs towards the reduction of 4-nitrophenol.[22] Considering the aforementioned aspects, the development of new stabilizers that can effectively stabilize metal NPs without blocking the active sites and the diffusion of the reactants and products to and from the metal surface is of paramount importance in catalysis.

Recently, we reported the first synthesis of fully water-soluble *ionic* polymeric carbon nitride, *i.e.*, potassium and sodium ion-containing poly(heptazine imide) (K,Na-PHI),[36] an ionic member of the polymeric carbon nitride family.[37–43] In aqueous solutions, the K,Na-PHI material can be fully dispersed in form of very small K,Na-PHI colloidal nanoparticles (hydrodynamic diameter ~10 nm) containing a large number of cyanamide and cyamelurate surface moieties, resulting in highly stable *quasi*-homogeneous solutions of K,Na-PHI with no gelation or precipitation over several months.[36] Given the unique features of K,Na-PHI (*i.e.*, water solubility, chemical stability, and ionic nature), we hypothesized that water-soluble K,Na-PHI might open a completely new and attractive possibility to stabilize catalytically active metal NPs. While various promising properties of ionic carbon nitrides, such as their photocatalytic activity and charge storage properties, are well established,[36,37,39,40,44–47] the use of ionic carbon nitrides as stabilizers has not been reported so far. In this contribution, we demonstrate, for the first time, the ability of K,Na-PHI to effectively stabilize ultrafine Au NPs (<3 nm). The stabilized Au NPs exhibit very high catalytic activity in the selective reduction of 4-nitrophenol (4-NP) to 4-aminophenol (4-AP) using $NaBH_4$ as a reducing agent (Fig. 1), a widely used model reaction for evaluating the catalytic activity of nanocatalysts in aqueous media.[22,23,48,49] Moreover, they show robust stability against agglomeration and excellent dispersibility for at least 2 months, as well as excellent accessibility in solution, as demonstrated by turnover frequencies superior to "naked" Au nanoparticles stabilized solely by excess BH_4^- anions. The stabilization effect of K,Na-PHI is elucidated using a comparative analysis employing different structural units of K,Na-PHI (cyanurate, melonate, and cyamelurate) and *ab initio* theoretical calculations, and the dominant role of functionalized heptazine moieties for the stabilization of Au NPs is discussed.

Experimental procedures and computational details

All experimental procedures and computational details are provided in the ESI.†

Results and discussion

Effect of the proposed stabilizers on Au NPs

Water-soluble K,Na-PHI has various functional groups attached to the heptazine units. Our structural analyses and theoretical calculations proposed that K,Na-PHI is characterized by a decreased number of terminal NH_x-groups, as compared to conventional, water-insoluble PCN, that are exchanged with cyamelurate and melonate moieties.[36] Furthermore, an incomplete condensation of the PCN precursor might result in the formation of triazine species within the polymer. Therefore, to obtain a deeper insight into the possible interactions between the Au NPs and K,Na-PHI, we also studied the stabilization effect of potassium melonate (KMel), potassium cyamelurate (KCya), and potassium cyanurate (KCA)

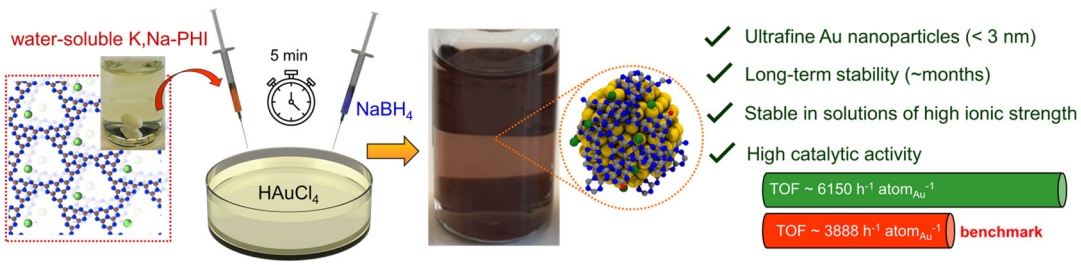

Fig. 1 Concept of effective stabilization of ultrafine Au nanoparticles using water-soluble ionic carbon nitride. The Au NPs are readily obtained by the addition of water-soluble K,Na-PHI into an aqueous solution of $HAuCl_4$ and subsequent reduction by sodium borohydride. The resulting ultrafine Au NPs (size <3 nm) are stable over several months even in solutions of high ionic strength and outperform benchmark "naked" Au NPs stabilized solely by excess $NaBH_4$ in a model catalytic reaction (selective reduction of 4-nitrophenol to 4-aminophenol using $NaBH_4$ as a reducing agent).

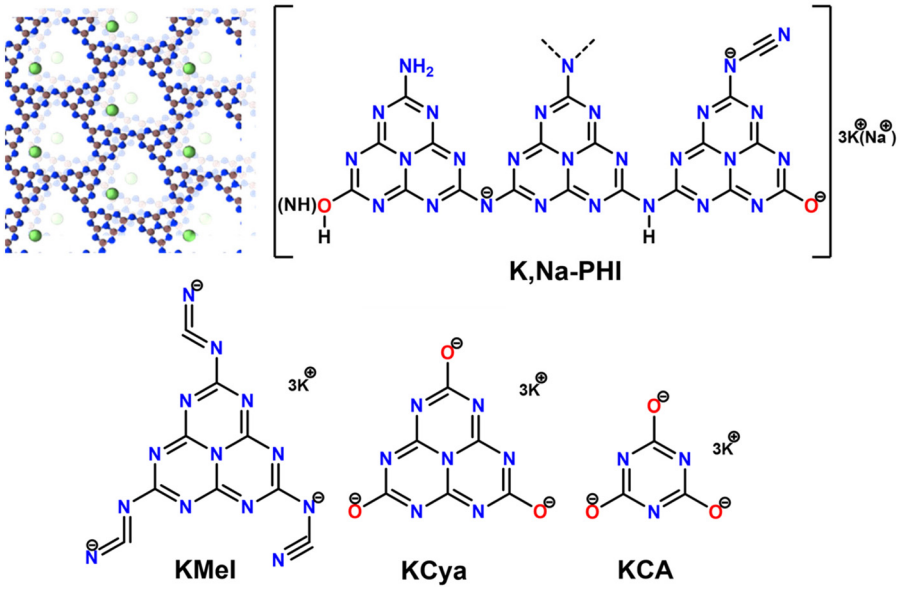

Fig. 2 Stabilizers used in the comparative analysis of the synthesis and catalytic activity of Au NPs. For K,Na-PHI both the typical 3D ionic carbon nitride structure comprising stacks of 2D heptazine-based networks and K^+ and Na^+ cations as well as a schematic structure highlighting the presence of charged surface moieties (*e.g.*, cyanamide and cyamelurate) is shown. For spectroscopic characterization (FTIR and NMR) see ESI, Fig. S1.†

at different concentrations (Fig. 2). For all the proposed stabilizers, $NaBH_4$ was used as a reducing agent for the synthesis of AuNPs. Notably, it is well established that the excess $NaBH_4$ can electrostatically stabilize even very small (~5 nm) colloidal Au NPs without any additional stabilizing agent.[50] Therefore, the "naked" (*i.e.*, ligand-free) Au NPs stabilized by excess $NaBH_4$ represent an ideal benchmark for comparative investigations of the effect of the proposed stabilizers on the size, long-term stability, and catalytic activity of Au NPs. This choice is further substantiated by the fact that though also other weakly binding ligands (*e.g.*, citrate) do allow for good accessibility of active sites on the Au nanoparticle surface, they are typically not able to stabilize Au NPs with sizes below 10 nm when using $NaBH_4$ as a reducing agent,[51–53] prohibiting thus comparative studies in the ultrafine size regime.

A 10-fold excess of $NaBH_4$ with respect to $HAuCl_4$ was selected as the optimum molar ratio of $NaBH_4$: $HAuCl_4$ to produce the benchmark ligand-free Au NPs (denoted as **Au10**) without agglomeration (for details see ESI 2.1†). For a systematic and realistic comparison, the same optimum $NaBH_4$ concentration was also used to fabricate Au NPs in the presence of K,Na-PHI and its monomeric constituents (KMel, KCya, and KCA). In general, the AuNPs stabilized by different concentrations of $NaBH_4$, K,Na-PHI, KMel, KCya, or KCA exhibit different colours and different electronic absorption properties, which is related to their different sizes and the differently pronounced surface plasmon resonance (SPR) effects (see ESI, Fig. S2 and S3,† and the detailed discussion of the optimization studies in ESI 2.1†). For a representative overview, Fig. 3 compares the UV-vis electronic absorption spectra and optical images as well as the average hydrodynamic diameters of **Au10**, **K,NaPHI2**, **KMel0.3**, **KCya0.3**, **KCA0.3** (the sample designations reflect the molar stabilizer : $HAuCl_4$ ratios; for details see ESI, Table S1†) that were obtained at the optimum concentrations for each stabilizer with respect to the smallest achievable size of stable NPs. As presented in Fig. 3a, the SPR peak of Au NPs stabilized by monomeric heptazine-based stabilizers (**K,NaPHI2**, **KMel0.3**, and **KCya0.3**) is less intense and broader than in the case of triazine-based stabilizers (**KCA0.3**) and **Au10**. Moreover, **K,NaPHI2** exhibits a considerably broader band with no discernible plasmonic feature at all, suggesting that most Au NPs are below ~5 nm in size.[54] These trends are consistent with the measurements of the hydrodynamic diameter using dynamic light scattering (DLS, Fig. 3b). In particular, the Au NP samples characterized by a relatively sharp and intense SPR peak show larger hydrodynamic diameters, indicating a larger particle size. More importantly, the inset of Fig. 3b demonstrates that **K,NaPHI2** possesses a very narrow hydrodynamic diameter distribution (3.0 ± 0.6 nm) as compared to other samples. These observations suggest that, although all the investigated triazine- and heptazine-based compounds can stabilize Au NPs, the size as well as the size distribution of the particles strongly depend on the polymerization degree of the stabilizer.

Zeta potential (ζ-potential) is the electric potential (Galvani potential) at the shear plane (*i.e.*, at the interface separating the mobile fluid from the fluid that remains attached to the NP surface), and represents an important indicator of the stability of colloidal suspensions by electrostatic repulsion forces. ζ-Potential is normally influenced by the nature of the NPs and the dispersion medium.[55] We measured the ζ-potential of the prepared suspensions of the Au NPs at the native pH value after dialysis against water to remove the excess $NaBH_4$ hydrolysis products. **Au10** displays a negative

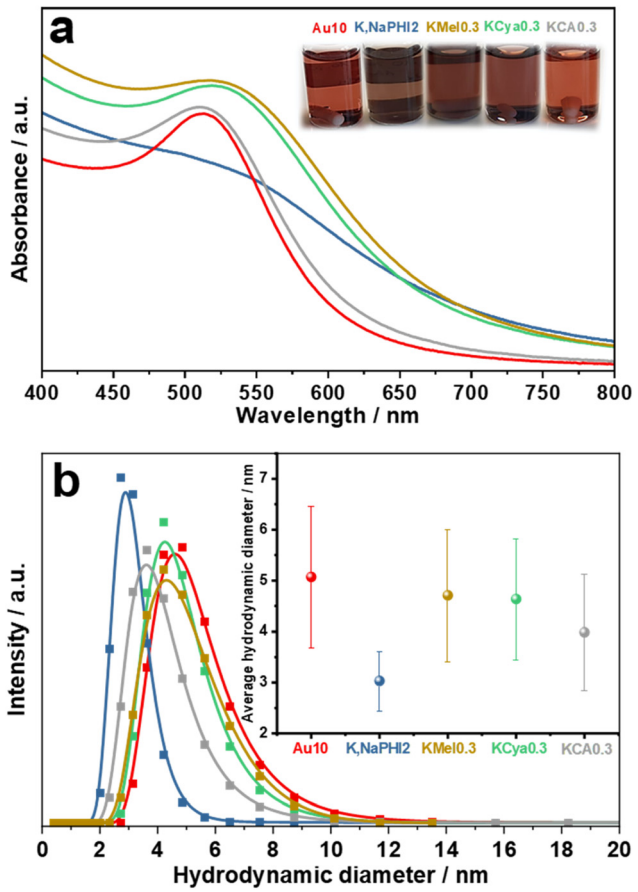

Fig. 3 Optical properties and hydrodynamic diameter of Au NPs: (a) UV-vis electronic absorption spectra and (b) hydrodynamic diameter data determined from the dynamic light scattering (DLS) of **Au10**, **K,NaPHI2**, **KMel0.3**, **KCya0.3**, and **KCA0.3**. The inset in (a) shows the optical images of the samples; the inset in (b) shows the average hydrodynamic diameters. The samples were measured after 1 day of their synthesis. The error bars were constructed as +/− the double of standard deviation (95% confidence interval).

ζ-potential value of −32 ± 1 mV (pH 6.8) because the surface of AuNPs is surrounded by a layer of BH_4^- or $B(OH)_4^-$. Similarly, **K,NaPHI2**, **KMel0.3**, **KCya0.3**, and **KCA0.3** show comparable negative ζ-potential values of −32 ± 2 (pH 6.0), −30 ± 1 (pH 5.7), −31 ± 1 (pH 5.5), and −32 ± 1 mV (pH 5.6), respectively, due to the negativity charged surface moieties (*e.g.*, cyanamide and cyamelurate) of heptazine and triazine-based stabilizers (see Fig. 2). The observed values of ζ-potential of *ca.* −30 mV are in line with the very good stability of NPs.[56]

Next, we analyzed the as-prepared samples using scanning transmission electron microscopy (STEM) as well as high-resolution transmission electron microscopy (HRTEM). The (S)TEM images of **Au10**, **K,NaPHI2**, **KMel0.3**, **KCya0.3**, and **KCA0.3** are shown in Fig. 4. The produced Au NPs with the proposed stabilizers have similar morphology, but the median diameter and the size distributions are different (Fig. 4f and ESI, Fig. S4†). The HAADF-STEM image of **Au10** shows the formation of dispersed Au NPs with a median diameter of around 5.6 nm, which is at least 2.5 times larger than that of **K,NaPHI2**, **KMel0.3**, and **KCya0.3**, but comparable to **KCA0.3**. Furthermore, the estimated particle size distributions reveal that **Au10** and **KCA0.3** have a broader size distribution than **K,NaPHI2**, **KMel0.3**, and **KCya0.3** (ESI, Fig. S4†). Notably, for samples stabilized by monomeric stabilizers (**KMel0.3**, **KCya0.3**, and **KCA0.3**) the observed trends are not fully in line with the trends of hydrodynamic diameters derived from the DLS measurements (compare Fig. 3b and Fig. 4f), which clearly indicates that the hydrodynamic diameter is strongly influenced by the nature of the stabilizer. Most importantly, in contrast to Au NPs stabilized by $NaBH_4$ only (**Au10**) or by cyanurate (**KCA0.3**), only K,Na-PHI (**K,NaPHI2**) and the monomeric *heptazine*-based stabilizers (**KMel0.3**, and **KCya0.3**) provide Au NPs in the ultra-small regime (sub-3 nm). The median diameter of Au NPs stabilized by K,Na-PHI is ~1.7 nm. This size is larger than the estimated cavity size of pol(heptazine imides) (~0.78 nm;[57] for a schematic representation of heptazine cages see ESI Fig. S5†), indicating that Au NPs are not confined in the heptazine cages.

X-ray photoelectron spectroscopy (XPS) analyses were performed to identify the oxidation state of gold and the chemical composition of **Au10**, **K,NaPHI2**, **KMel0.3**, **KCya0.3**, and **KCA0.3**. As shown in Fig. 5, the two distinct peaks centered at 83.6 and 87.3 eV correlate to the spin–orbit doublet of Au $4f_{7/2}$ and $4f_{5/2}$, respectively, demonstrating the presence of metallic Au in the samples.[58] Interestingly, the stabilizers do not significantly affect the binding energy of Au $4f_{7/2}$ and Au $4f_{5/2}$ electrons (ESI, Table S2†), which implies that the stabilizer moieties interact rather weakly with the surface of the Au NPs, most likely *via* electrostatic attractions.

Long-term stability of Au NPs

First, we have investigated the long-term stability of the produced Au NPs against agglomeration under ambient storage conditions. Fig. 6 compares the UV-vis spectra and average hydrodynamic diameters of **Au10**, **K,NaPHI2**, **KCya0.3**, and **KCA0.3** over time. The SPR peak and hydrodynamic diameter of **Au10**, **K,NaPHI2**, and **KCya0.3** did not change significantly over 28 days, indicating high stability against agglomeration (Fig. 6a–c and e). In contrast, **KCA0.3** tends to agglomerate over time, as demonstrated by a sharper SPR peak and larger hydrodynamic diameter after 28 days. Notably, **Au10** possesses a higher tendency to agglomeration after about two months of storage, as indicated by the red-shift of the SPR peak by about 10 nm (inset of Fig. 6a) and the larger hydrodynamic diameter (Fig. 6e). It should be noted that the **K,NaPHI2** shows outstanding stability for at least two months, suggesting that K,Na-PHI is a remarkably effective stabilizer that endows the Au NPs with long-term stability.

Further, we investigated the influence of various concentrations of K,Na-PHI, KCya, and KCA stabilizers on the stability of Au NPs over time (see ESI, Fig. S8a–c and Fig. S9a–f†). Notably, no changes in the UV-vis spectra of the Au NPs stabilized by K,Na-PHI are observed after two months of storage for all the investigated concentrations (ESI, Fig. S8a†). The DLS

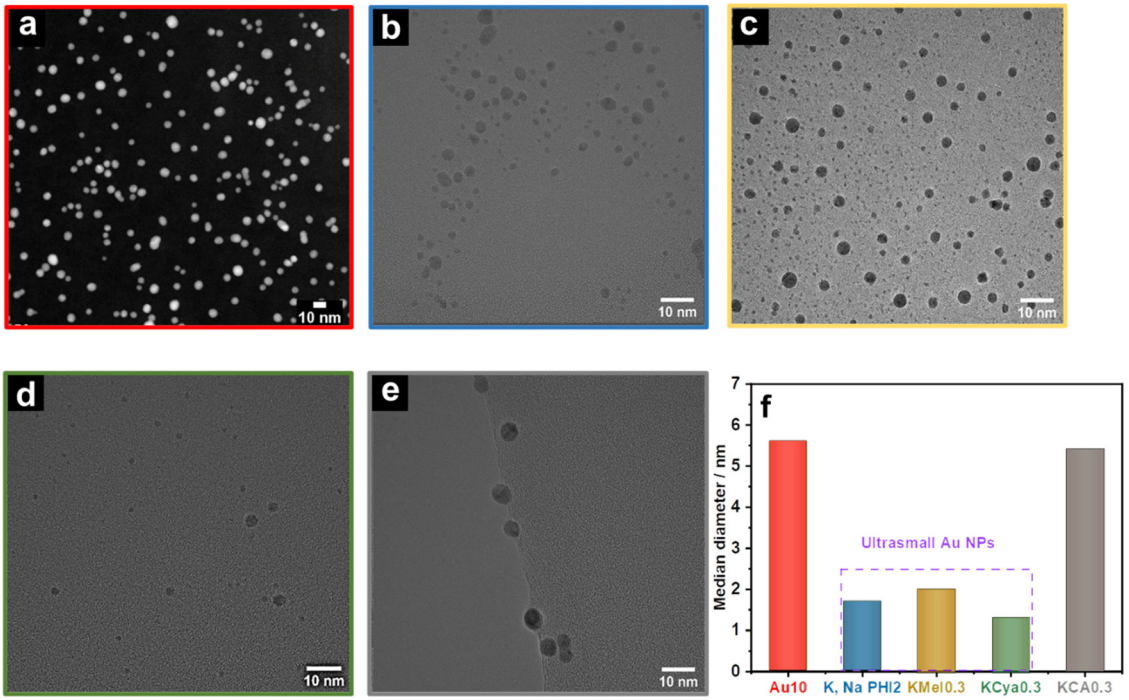

Fig. 4 Size of NPs. HAADF STEM image of (a) **Au10**, and HRTEM images of (b) **K,NaPHI2**, (c) **KMel0.3**, (d) **KCya0.3**, and (e) **KCA0.3**, and their corresponding median diameter (f) derived from the TEM images (for size distribution histograms see ESI, Fig. S4†).

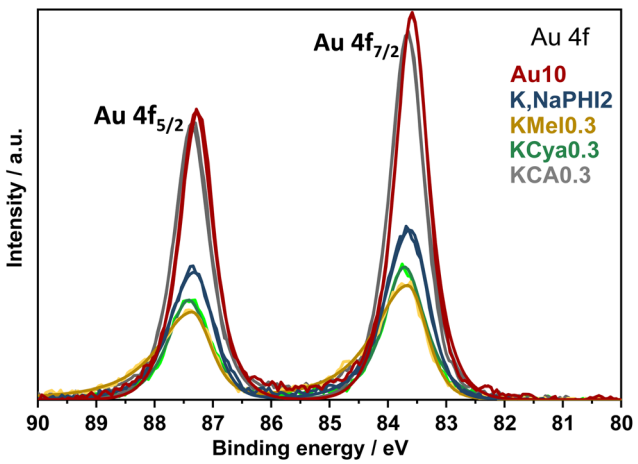

Fig. 5 XPS analysis. High-resolution Au 4f XP spectra of **Au10**, **K,NaPHI2**, **KMel0.3**, **KCya0.3**, and **KCA0.3**. Further details regarding the XPS analysis of all samples are provided in ESI, Fig. S6 and S7.†

measurements demonstrate that the hydrodynamic diameter of Au NPs increases as a function of K,Na-PHI concentration (ESI, Fig. S9a and b†), which suggests that the hydrodynamic diameter is strongly influenced not only by the nature of the stabilizer but also by its amount. Moreover, all the K,Na-PHI stabilized Au NPs are highly dispersed and stable for at least two months except for **K,NaPHI5**, where the hydrodynamic diameter is slightly increasing over time, possibly due to an excessively high amount of the stabilizer. In the case of KCya and KCA-stabilized Au NPs, the stability of the produced Au NPs decreases over time, especially when the molar ratios of the stabilizer with respect to $HAuCl_4$ are ≥10 (see ESI, Fig. S8b, c,† and Fig. 9c–f). The increased tendency to the agglomeration of Au NPs at higher concentrations of KCya and KCA is most likely due to the shorter Debye-length of the electrical double layer as a consequence of the higher ionic strength.[59,60]

Stability of Au NPs at high ionic strength

The stability of metal nanoparticles in solutions of high ionic strength is crucial for their application in catalysis and biology.[61] Therefore, the effect of ionic strength on the stability of **Au10**, **K,NaPHI2**, **KMel0.3**, **KCya0.3**, and **KCA0.3** was investigated by the addition of NaCl at different concentrations (0.001, 0.01, and 0.1 M). The corresponding optical images and average hydrodynamic diameter of the samples are shown in Fig. 7. Remarkably, **K,NaPHI2** and **KMel0.3** are stable and agglomeration-free for at least 6 days even in the presence of 0.1 M NaCl. In contrast, **Au10**, **KCya0.3**, and **KCA0.3** tend to agglomerate over time in the presence of 0.001 and 0.01 M NaCl, as indicated by a larger hydrodynamic diameter and darker brown colour after 6 days of storage. Moreover, the optical images of these samples demonstrate a complete agglomeration in the presence of 0.1 M NaCl after less than 24 h (Fig. 7a). Similar behaviour is well-known for Au NPs stabilized by electrostatic repulsion, such as citrate-capped Au NPs, and can be ascribed to the increased screening of the surface charge and compression of the double layer, resulting in a more attractive particle–particle van der Waals interaction

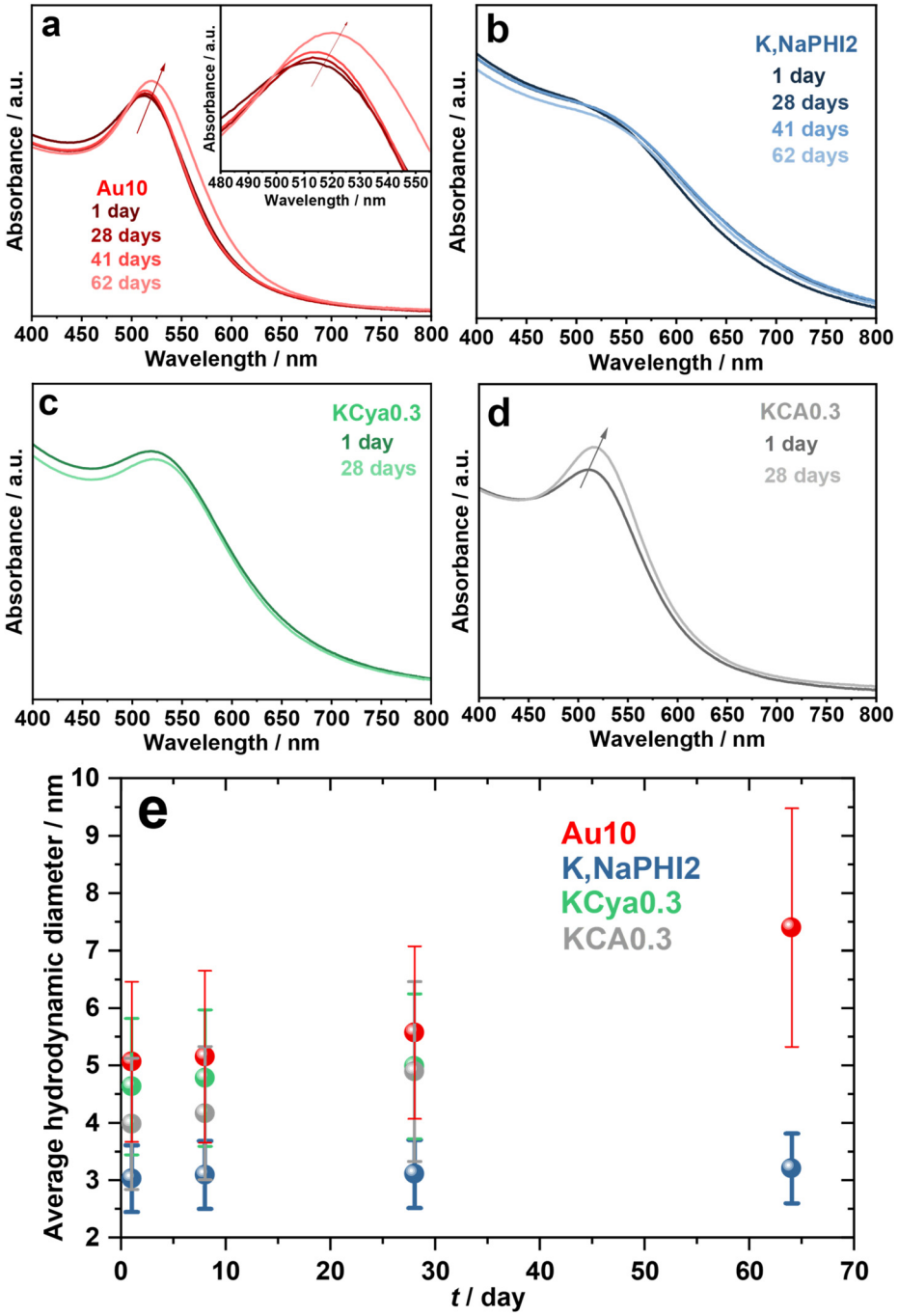

Fig. 6 Long-term stability. (a–d) UV-vis electronic absorption spectra and (e) average hydrodynamic diameter determined from the DLS results of **Au10**, **K,NaPHI2**, **KCya0.3**, and **KCA0.3** as a function of storage time under ambient conditions.

and agglomeration.[62–64] In this context, the strongly enhanced stability of Au NPs stabilized by K,Na-PHI and KMel can be likely explained by the ability of these stabilizers to act as a hydrated protective layer that is, due to the more pronounced delocalization of charges (see the discussion below), less prone to the double layer compression effects and thus more effectively diminishes the attractive forces between the particles at high ionic strength.[59]

Stability of Au NPs at elevated temperature

The thermal stability of colloidal nanoparticles is of paramount importance for practical applications.[65,66] Therefore, **Au10**, **K,NaPHI2**, **KMel0.3**, **KCya0.3**, and **KCA0.3** were heated at 85 °C for 4 h, 8 h, 24 h, 48 h, and 72 h to determine the thermal stability. **Au10** and **KCA0.3** exhibit a notable broadening of the plasmon band, along with a slight red shift of the

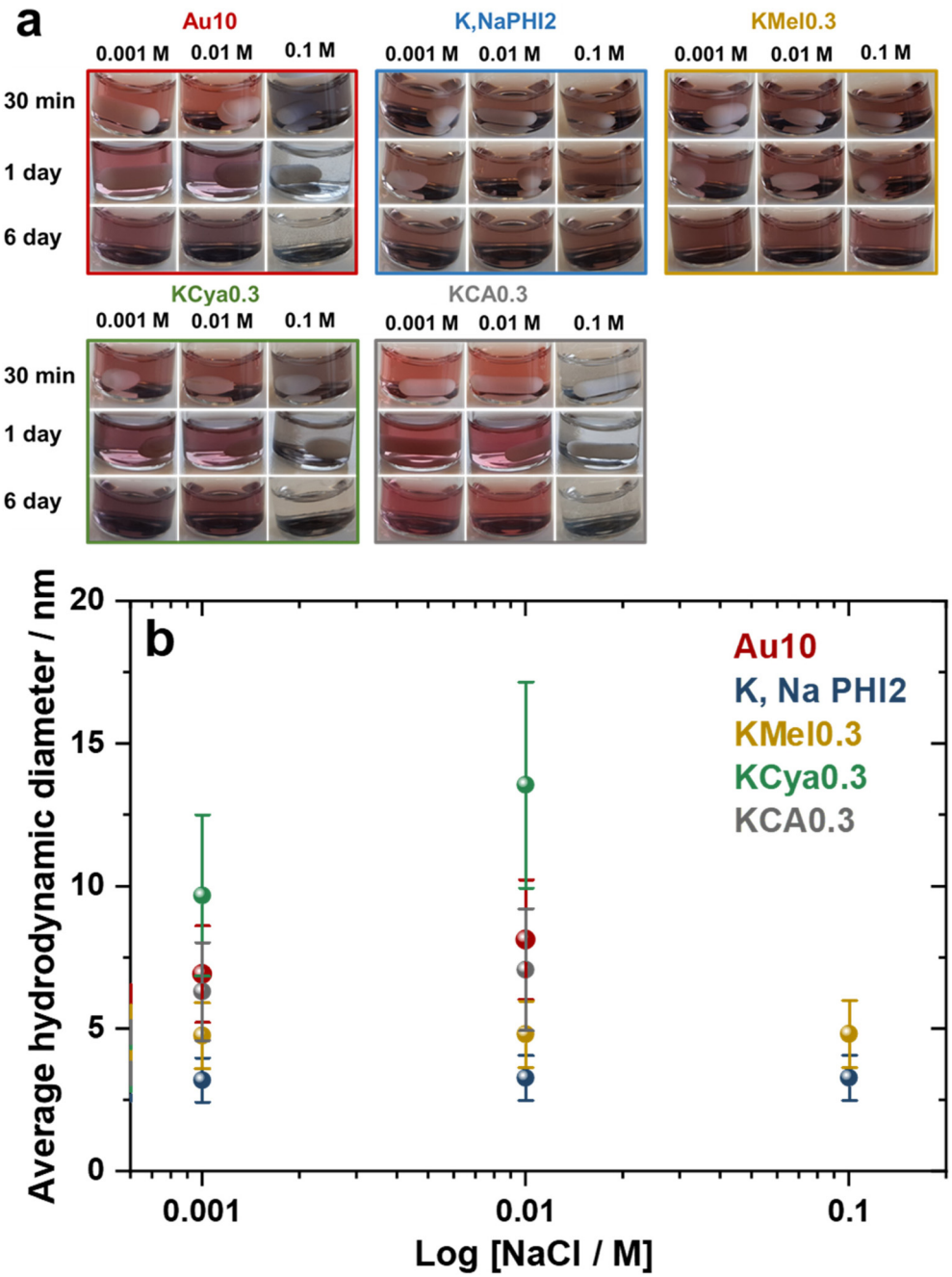

Fig. 7 Stability at high ionic strength. (a) Optical images of **Au10**, **K,NaPHI2**, **KMel0.3**, **KCya0.3**, and **KCA0.3** in the presence of different concentrations of NaCl and (b) the corresponding average hydrodynamic diameter measured 6 days after the addition of NaCl.

maximum, after heating at 85 °C for 4 h and 48 h, respectively (ESI, Fig. S10a and e†). This indicates that at higher temperatures, the nanoparticles experience growth and aggregation, resulting in larger particle sizes due to nanoparticle coalescence.[67] In comparison, the SPR peak of **K,NaPHI2**, **KMel0.3**, and **KCya0.3** did not change considerably after heating at 85 °C even after 72 h, revealing excellent dispersion stability against heating (ESI, Fig. S10b–d†). These results highlight the beneficial effects of the heptazine-based stabilizers that are assumed to form a hydrated protective layer that effectively prevents nanoparticle coalescence and further growth during heating.

Effect of the reductant-derived impurities on the Au NPs stability

It is known that the stabilization mechanism of pristine Au NPs (**Au10**) stabilized by the excess of $NaBH_4$ relies on the formation of a layer (incorporating water molecules) of anions

(BH_4^-, $B(OH)_4^-$, Cl^-) and cations (Na^+; in a second layer) formed during the reduction of $HAuCl_4$ by $NaBH_4$ on the surface of Au NPs.[50] Hence, to evaluate the true stabilization ability of K,Na-PHI, the prepared suspensions of the Au NPs were dialyzed against water to remove the $NaBH_4$ hydrolysis products. The results unambiguously show that K,Na-PHI can efficiently stabilize ultrafine AuNPs also in the *absence* of the $NaBH_4$ hydrolysis products; for details see ESI, Fig. S11 and S12,† as well as Tables S3 and S4.†

Stabilization mechanism

The studied stabilizers K,Na-PHI, KMel, KCya, and KCA are water-soluble ionic compounds bearing negatively charged functional groups (see Fig. 2). In particular, K,Na-PHI consists of a poly(heptazine imide) network incorporating, apart from NH and $-NH_2$ groups or uncondensed NH_x-including triazine species, also terminal cyanamide N–C≡N^- and cyamelurate C–O^- functional groups. We have reported that the dissolved K,Na-PHI has a zeta potential of −31 mV at a pH of 7.5,[36] confirming the negatively charged surface under our reaction conditions. The presence of the negatively charged functional groups on the stabilizers allows for electrostatic stabilization and solubilization of Au NPs in water. The stabilization of the NPs by repulsive electrostatic interactions originates from a diffuse double layer at the surface of NPs coated with charged molecules. Presumably, K,Na-PHI, KMel, KCya, and KCA establish a hydrophilic protective layer around the growing metal nuclei that is permeable to tetrachloroaurate ions (to allow for self-limiting growth) while preventing the diffusional coupling of the particles. A representative model for the electrostatic stabilization of Au NPs by K, Na-PHI is shown in Fig. 8. These considerations are mainly based on the TEM and XPS results revealing that (i) the particle size of Au NPs stabilized by K,Na-PHI is larger than the estimated cavity size of heptazines (ESI, Fig. S5†), excluding the confinement of Au NPs into the heptazine cages, and (ii) the presence of K,Na-PHI does not affect the binding energy of Au $4f_{7/2}$ and Au $4f_{5/2}$ electrons of the Au (0) species, revealing that the stabilizer functional groups only weakly interact with the surface of the Au NPs. Although the stabilization of the Au NPs in water is conditioned by the charged functional groups, the size of the obtained Au NPs depends mostly on the employed stabilizer, *i.e.*, on the monomeric unit and the polymerization degree. Most notably, as compared to the triazine-based stabilizer (KCA), the stabilizers containing heptazine units (K,Na-PHI, KMel, KCya) lead to smaller Au NPs which also exhibit better stability (except for cyanurate) in high ionic strength electrolytes.

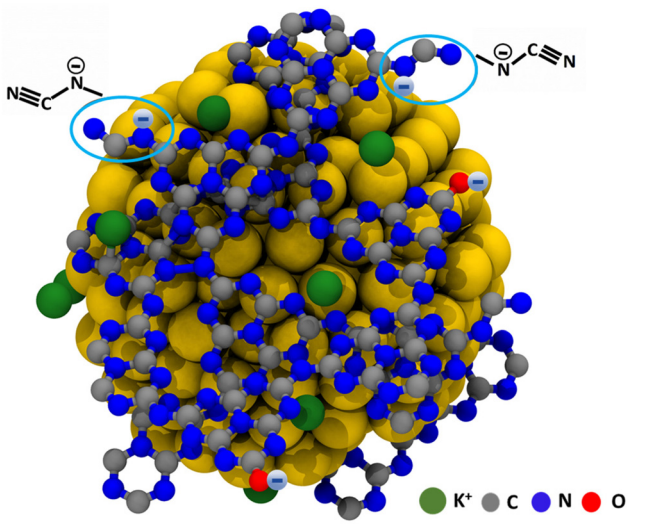

Fig. 8 Schematic representation of the stabilization of Au NPs by K,Na-PHI.

We hypothesized that these beneficial effects of larger heptazine-based stabilizers might be due to the larger charge delocalization in the aromatic system, resulting in more effective electrostatic stabilization of Au NPs which are typically positively charged.[50] To obtain further insight into the stabilization mechanism, we performed density functional theory (DFT) calculations to find the optimized geometry of KCA, KCya, and KMel structures and to investigate the impact of the conjugation size, negatively charged cyamelurate or cyanamide functional groups, and the nature and number of counterions (Fig. 9). Particularly, we modelled the structures with a different number of counterions based on the assumption that the counterions initially stabilize the carbon nitride species and may detach after the stabilization of Au NPs. In addition, we performed a Fukui function analysis of the carbon nitride species to gain a deeper understanding of the stabilization mechanism of Au NPs.[68–71] This analysis provides an estimate of the expected interaction between the stabilizer and Au-NP without the need to directly include the extended Au-NP (having a broad size and shape distribution) into the simulation. More specifically, the electron density of the f^- Fukui function of the carbon nitride represents the electron density for the electrophilic attack from the Au NPs (Fig. 9). The optimized geometries of the carbon nitride species functionalized by the oxygen-containing cyamelurate groups (CA and Cya) reveal a structural out-of-plane deformation near the cyamelurate groups when the counterions are absent. However, in the presence of the counterions, the structures become more planar. In this context, it should be mentioned that the out-of-plane structural distortion translates into a breaking of the π-electron conjugation, which effectively reduces the size of electron delocalization. On the other hand, the cyanamide (NCN^-)-functionalized species (melonate) tends to retain an in-plane structure. The presence of potassium counterions renders the structure even more planar, resulting in an extension of the electron conjugation as compared to the situation without the counterions. Therefore, the primary role of the counterions (potassium) can be understood as facilitating the flattening of the structures with functional groups. Specifically, the electron densities of f^- Fukui functions reveal that the presence of counterions causing the structural flattening leads to an alignment of the directional orbitals from the previously distorted structure into perpendicular π-orbitals within the flat structure. This orbital alignment translates into

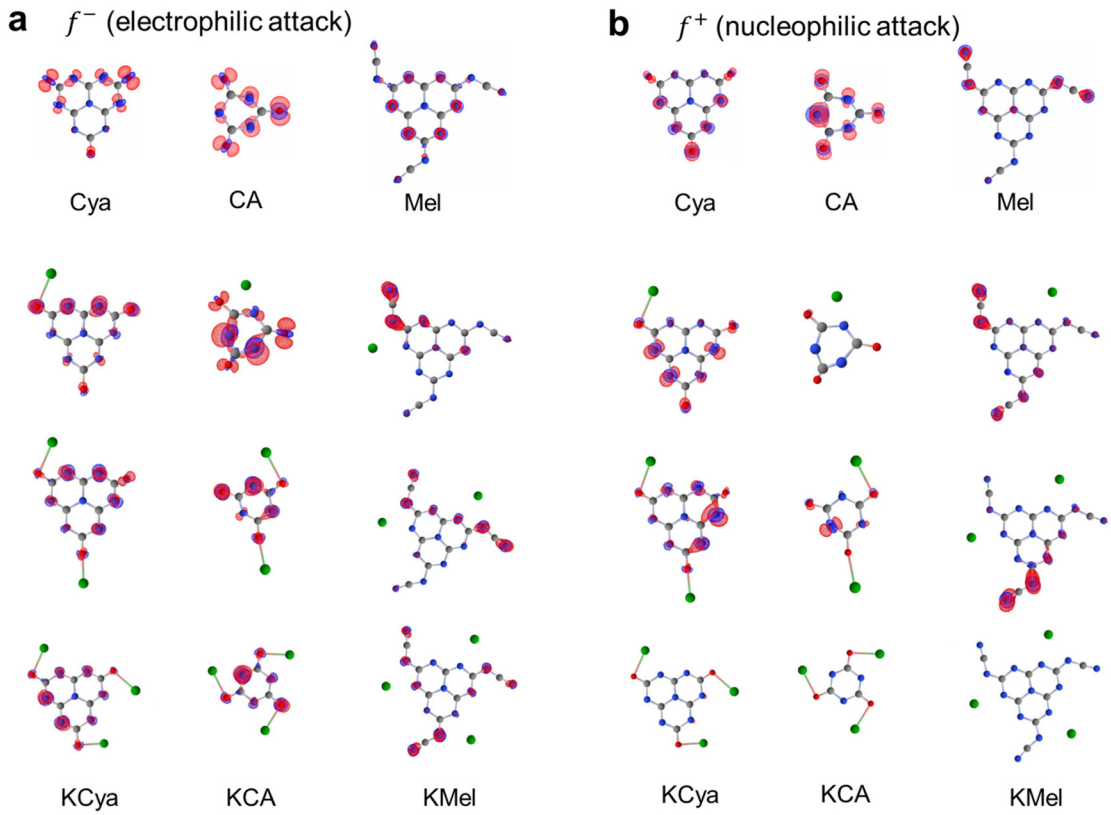

Fig. 9 Theoretical calculations. The electron density from Fukui function (a) negative f^- and (b) positive f^+. The electron density shows the potential frontier reactive site for the respective carbon nitride species. The isosurface value of the electron density is fixed to 0.005787 e Å^{-3} over the structures. The structure is illustrated without the cation (top) and with the different numbers (1–3) of potassium cations (bottom). The blue, the gray, and the green balls stand for N, C, and K atoms, respectively.

an extension of the delocalized electron cloud to the functional groups, facilitating thus the stabilization of the positive surface of Au NPs. The effectiveness of the extended π orbitals in stabilizing Au NPs is supported by the experimental observation that the stabilization (in terms of size and long-term stability) of Au NPs by the structurally more distorted KCA is similar to the case of stabilization solely by $NaBH_4$, while the flatter carbon nitride species, such as KCya, K,Na-PHI, and KMel, can effectively stabilize Au NPs smaller than 3 nm in size (see Fig. 4f and the histograms in ESI, Fig. S4†). In other words, these results suggest that the more effective stabilization of Au NPs by KCya, K,Na-PHI, and KMel as compared to KCA can be attributed to the availability of a delocalized electron cloud with a size equivalent to or larger than the heptazine moiety. In addition, from the analysis of the condensed Fukui function (for details see section 1.5. in ESI†), also known as the dual descriptor, we conclude that this phenomenon is a result of the synergistic effects of the functional groups and the counterions (Fig. 10). The condensed Fukui function describes the local reactivity per atom, and its value is negative at sites prone to the electrophilic attack from an electrophile, and positive at sites preferable for the nucleophilic attack.[68–73] Notably, the condensed Fukui functions for all atoms in structures with the same number of K^+ counterions as the number of functional groups yield all negative values, which corroborates their ability to effectively stabilize the electrophilic Au NPs (Fig. 10). In contrast, the pristine (non-ionic, non-functionalized) heptazine and triazine moieties show positive values of the condensed Fukui functions despite their positive net charge (Fig. S13 and S14 in ESI†), which highlights the significance of the presence of the counterion-balanced cyamelurate and cyanamide functional groups in ionic carbon nitride for the effective stabilization of Au NPs.

Catalytic performance

It is known that strongly interacting stabilizing agents might block the utilization and accessibility of the active sites on the surface of catalytic metal NPs, resulting in catalyst deactivation/poisoning.[22,35] However, the stabilizers that *electrostatically* stabilize Au NPs typically do not interfere significantly with the mass transport processes towards the catalytic surface, thus allowing for high diffusion rates of the reactants and products without completely blocking the active sites.[22,23] As a proof of concept, the catalytic activity of **K,NaPHI2**, **KMel0.3**, **KCya0.3**, and **KCA0.3** was evaluated in the selective reduction of 4-nitrophenol (4-NP) to 4-aminophenol (4-AP) by $NaBH_4$, using the "naked" Au NPs electrostatically stabilized by excess $NaBH_4$ (**Au10**) as a benchmark. The catalytic activity

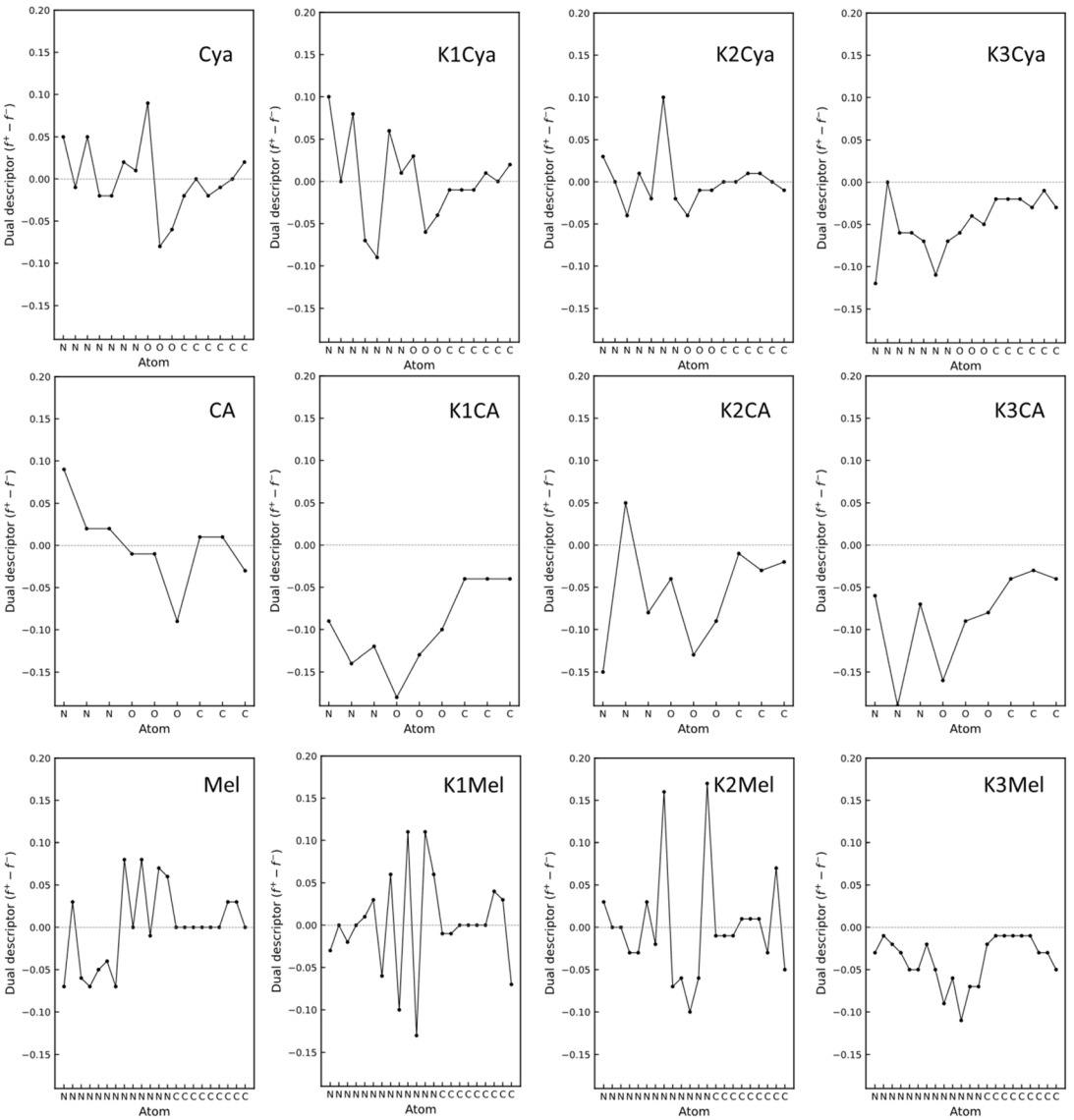

Fig. 10 Condensed Fukui functions. The dual descriptor of the carbon nitride species (Cya, CA, and Mel) in the presence of the different numbers of potassium cations. The negative value corresponds to the electrophilic attack site and the positive value corresponds to the nucleophilic attack site. The values for potassium ions have been excluded in order to emphasize the variations in other atoms. All values, including those for potassium ions, are shown in Table S5 in ESI.†

of all investigated samples was evaluated one day after their synthesis. The catalytic hydrogenation of nitroarenes has been extensively employed as a model reaction to evaluate the activity of Au NP catalysts, and it has the advantage of easy monitoring by UV-vis spectroscopy.[16,22,23,58] As the reaction proceeds after the addition of the catalyst, the absorption peak at 400 nm decreases, while the absorption peak at 300 nm is increasing, showing the conversion of 4-NP to 4-AP (Fig. 11a). The time dependence of the relative absorbance (A_t/A_0%) of the 4-nitrophenolate peak at 400 nm in the presence of **Au10**, **K,NaPHI2**, **KMel0.3**, **KCya0.3**, or **KCA0.3** is shown in ESI, Fig. S15a,† where A_t and A_0 represent the absorbance at the reaction time t and at time t = 0, respectively. An important feature of the reduction of 4-NP catalyzed by ligand-stabilized nanoparticles is the induction period, an initial time interval needed until the reaction takes place.[23] The induction period is related to either the formation of a diffusion pathway through the ligand shell on the NP surface or the restructuring of the NP surface induced by the adsorbed reactant molecules.[22,23,74,75] Interestingly, very short (~2–20 s) induction times are observed for all investigated materials except for **KCA0.3** (~45 s; Fig. S15a†), which indicates that especially the heptazine-based stabilizing agents can *both* effectively stabilize the Au NPs *and* allow for fast diffusion of reactants and products needed for effective surface catalysis.

The rate constants (Fig. 11b) were determined by fitting the data from Fig. S15a† to a pseudo-first-order kinetic model concerning the concentration of 4-NP (Fig. S15b†). The turnover

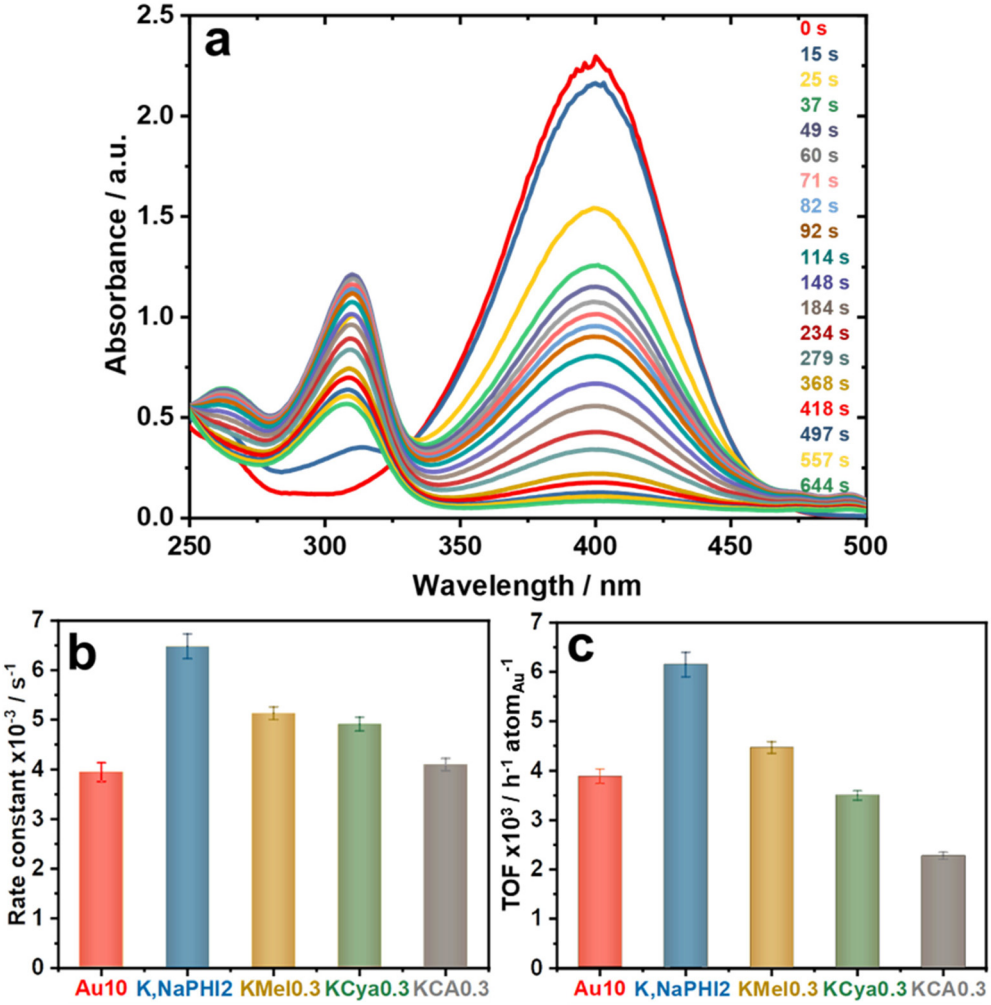

Fig. 11 (a) UV-vis electronic absorption spectra recorded during the reduction of 4-NP in the presence of **K,NaPHI2** catalyst and the calculated (b) rate constant and (c) TOF values for **Au10**, **K,Na PHI2**, **KMel0.3**, **KCya0.3**, and **KCA0.3**. Experimental conditions: 0.1 mL $NaBH_4$ (2.16 mol L^{-1}), 0.3 mL 4-NP (1.2×10^{-3} mol L^{-1}), and 2.5 mL distilled water were mixed into a cuvette at ambient conditions. Then, the UV-Vis spectrum was recorded, followed by the addition of 0.025 mL of AuNP catalyst (1.14 mg L^{-1}) and shaking quickly the cuvette before recording the subsequent spectra.

frequencies (TOF) for investigated samples (Fig. 11c) were calculated using the linear range of substrate conversion at the beginning of the reaction, taking the end of the induction period as time 0. The TOF value is given with respect to one atom of Au, hence its unit is h^{-1} $atom_{Au}^{-1}$. The benchmark sample **Au10** has a TOF value of 3888 h^{-1} $atom_{Au}^{-1}$, which is comparable to the value reported in the literature.[50] Notably, the **K,NaPHI2** catalyst exhibits a remarkably high TOF value of 6149 h^{-1} $atom_{Au}^{-1}$, which is superior to TOFs of the benchmark **Au10** (3888 h^{-1} $atom_{Au}^{-1}$), **KMel0.3** (4464 h^{-1} $atom_{Au}^{-1}$), **KCya0.3** (3498 h^{-1} $atom_{Au}^{-1}$), and **KCA0.3** (2276 h^{-1} $atom_{Au}^{-1}$), as shown in Fig. 11c. The sample **KCA0.3**, comprising a triazine-based stabilizer, possesses the lowest TOF value, which is likely because KCA leads to larger Au NPs. Moreover, among the proposed stabilizers, KCA has the highest density of negatively charged groups where all carbons bear one negatively charged O^- group. Therefore, the AuNPs surface is likely crowded by the stabilizing molecules, partially blocking the surface catalytic activity. The outstanding catalytic performance of the Au NPs stabilized by K,Na-PHI can be, in our view, attributed to two main effects. Firstly, K,Na-PHI favours the formation of ultrasmall Au NPs, allowing for higher specific surface area and more optimal utilization of Au atoms. Secondly, the flexible and extended framework structure of the polymeric K, Na-PHI enables *both* effective stabilization *and* – at the same time – facilitates the diffusion of reactants and products to and from the surface of gold NPs. In this context, it should be noted that $NaBH_4$ at high concentrations is known to increase significantly the ionic strength and thus to induce aggregation of Au NPs.[76] Indeed, under our reaction conditions, both **Au10** and **K,NaPHI2** are prone to aggregation, as apparent by a blue shift of the SPR band (see ESI, Fig. S16†), which can be ascribed to a high concentration of $NaBH_4$ in the reaction solution as $NaBH_4$ is used in a large excess (~600 times the concentration of 4-NP, *i.e.* ~0.1 M). Higher stability against aggregation is expected to be achievable in catalytic reactions operating under optimized conditions with alternative reagents and/or at lower ionic strengths.

Conclusions

In this work, we demonstrate for the first time that water-soluble ionic (K^+ and Na^+ containing) polymeric carbon nitride (K,Na-PHI) can act as a facile, scalable, and highly effective stabilizer in the synthesis of highly catalytically active ultrafine (<3 nm) gold nanoparticles. In the selective reduction of 4-nitrophenol to 4-aminophenol by $NaBH_4$ employed as a model catalytic reaction, the K,Na-PHI-stabilized Au NPs not only outperform Au NPs stabilized by monomeric structural units of K,Na-PHI (cyanurate, melonate, cyamelurate), but their activity is even superior (TOF higher by the factor of ~1.6) to that of the benchmark "naked" (*i.e.*, ligand-free) Au NPs electrostatically stabilized by excess $NaBH_4$. These results suggest that K,Na-PHI can provide an effective electrostatic stabilization against the aggregation of Au NPs, without blocking the diffusion of the reactants and products to and from the active sites at the Au catalyst surface. A truly outstanding feature of our K,Na-PHI-stabilized Au NPs is their excellent stability both under ambient conditions (over at least two months), as well as under high ionic strength conditions (up to 0.1 M NaCl solutions) and at elevated temperatures (85 °C for at least 72 hours). Based on our experimental evidence and theoretical calculations, we propose that the strongly enhanced stability of Au NPs stabilized by K,Na-PHI can be explained by the ability of K,Na-PHI to act as a hydrated protective layer that is, due to the more pronounced delocalization of charges, less prone to the double layer compression effects and thus more effectively diminishes the attractive forces between the nanoparticles. Moreover, a detailed comparative study using different structural units of K,Na-PHI (cyanurate, melonate, cyamelurate) shows that in particular the presence of functionalized heptazine moieties allowing for better charge delocalization is crucial for the synthesis and more effective stabilization of small Au NPs. This is corroborated by theoretical DFT calculations of Fukui functions which reveal the beneficial effect of the counterion-balanced cyamelurate and cyanamide functional groups in the ionic carbon nitride on the orbital alignment and electron delocalization, resulting in more effective stabilization of Au NPs. Thus, this work establishes the ionic carbon nitrides (PHI) as alternative capping agents for nanocatalysts that enable effective stabilization without compromising surface catalysis. More generally, it opens up a route for further developments in utilizing PHI-based stabilizers for the synthesis of high-performance ultrafine nanoparticles, especially for applications in which both the stability and the effective transport of species between the interfacial region of nanoparticles and the environment is mandatory.

Author contributions

M.E., L.K., I.K., T.J., R.B. and D.M. conceived and supervised the project, J.L., M.E. and I.K. synthesised the materials, characterized them and performed catalytic experiments. C.N. and A.T. performed XPS investigation of the materials and analysed the results. R.L. and U.K. performed TEM-EDX analyses and processed the data. C.I. and T.J. performed the theoretical calculations. M.E. wrote the first draft of the manuscript, and M.E., J.L., C.I., I.K. and R.B. finalized the manuscript with inputs from all authors.

Data availability

All datasets related to this work are available from the repository: **https://doi.org/10.5281/zenodo.8130796**.

Conflicts of interest

There are no conflicts to declare.

Acknowledgements

This work was funded by the Deutsche Forschungsgemeinschaft (DFG, German Research Foundation) – Project No. 364549901 – TRR 234 CataLight (Projects B6, B7, B10, Z2) as well as JA 1972/27-1 and BE 5102/5-1 (Project No. 428764269). Computational resources were provided by the state of Baden–Württemberg through bwHPC and the German Science Foundation (DFG) under Grant No. INST 40/467-1 FUGG. C. N. and A. T. acknowledge financial support of the DFG through a research infrastructure grant INST 275/257-1 FUGG. I. K. acknowledges support by Spanish MCINN (PID2020-113558RB-C41), Gobierno del Principado de Asturias (IDI-2021-000048), and the Alexander von Humboldt Foundation through the Humboldt Research Fellowship.

References

1 N. Wang, Q. Sun and J. Yu, *Adv. Mater.*, 2019, **31**, 1803966.
2 X. Yang, J.-K. Sun, M. Kitta, H. Pang and Q. Xu, *Nat. Catal.*, 2018, **1**, 214–220.
3 Q. L. Zhu and Q. Xu, *Chem*, 2016, **1**, 220–245.
4 L. M. Liz-Marzán, *Langmuir*, 2006, **22**, 32–41.
5 M.-C. Daniel and D. Astruc, *Chem. Rev.*, 2004, **104**, 293–346.
6 V. Karthick, L. Kumar Shrestha, V. G. Kumar, P. Pranjali, D. Kumar, A. Pal and K. Ariga, *Nanoscale*, 2022, **14**, 10630–10647.
7 D. Jaque, L. Martínez Maestro, B. del Rosal, P. Haro-Gonzalez, A. Benayas, J. L. Plaza, E. Martín Rodríguez and J. García Solé, *Nanoscale*, 2014, **6**, 9494–9530.
8 O. J. H. Chai, Z. Liu, T. Chen and J. Xie, *Nanoscale*, 2019, **11**, 20437–20448.
9 H. T. K. Duong, A. Abdibastami, L. Gloag, L. Barrera, J. J. Gooding and R. D. Tilley, *Nanoscale*, 2022, **14**, 13890–13914.
10 M. E. King, M. V. Fonseca Guzman and M. B. Ross, *Nanoscale*, 2022, **14**, 602–611.

11 C. Spedalieri and J. Kneipp, *Nanoscale*, 2022, **14**, 5314–5328.
12 C. Adler, D. Mitoraj, I. Krivtsov and R. Beranek, *J. Chem. Phys.*, 2020, **152**, 244702.
13 J. Yang, M. Yuan, D. Xu, H. Zhao, Y. Zhu, M. Fan, F. Zhang and Z. Dong, *J. Mater. Chem. A*, 2018, **6**, 18242–18251.
14 R. R. Nasaruddin, T. Chen, N. Yan and J. Xie, *Coord. Chem. Rev.*, 2018, **368**, 60–79.
15 L.-W. Guo, P.-P. Du, X.-P. Fu, C. Ma, J. Zeng, R. Si, Y.-Y. Huang, C.-J. Jia, Y.-W. Zhang and C.-H. Yan, *Nat. Commun.*, 2016, **7**, 13481.
16 X. Gou, T. Liu, Y. Wang and Y. Han, *Angew. Chem., Int. Ed.*, 2020, **59**, 16683–16689.
17 H. Yang, Z. Yu, S. Li, Q. Zhang, J. Jin and J. Ma, *J. Catal.*, 2017, **353**, 256–264.
18 Y. Jiang, X. Zhang, X. Dai, W. Zhang, Q. Sheng, H. Zhuo, Y. Xiao and H. Wang, *Nano Res.*, 2017, **10**, 876–889.
19 B. Weng, K.-Q. Lu, Z. Tang, H. M. Chen and Y.-J. Xu, *Nat. Commun.*, 2018, **9**, 1543.
20 A. Mondal and N. R. Jana, *ACS Catal.*, 2014, **4**, 593–599.
21 Y. Wang, J. He, C. Liu, W. H. Chong and H. Chen, *Angew. Chem., Int. Ed.*, 2015, **54**, 2022–2051.
22 S. M. Ansar and C. L. Kitchens, *ACS Catal.*, 2016, **6**, 5553–5560.
23 R. D. Neal, R. A. Hughes, P. Sapkota, S. Ptasinska and S. Neretina, *ACS Catal.*, 2020, **10**, 10040–10050.
24 A. M. Alam and Y. S. Shon, *ACS Appl. Nano Mater.*, 2021, **4**, 3294–3318.
25 Q. L. Zhu and Q. Xu, *Chem*, 2016, **1**, 220–245.
26 J. A. Singh, S. H. Overbury, N. J. Dudney, M. Li and G. M. Veith, *ACS Catal.*, 2012, **2**, 1138–1146.
27 G. González-Rubio, J. Mosquera, V. Kumar, A. Pedrazo-Tardajos, P. Llombart, D. M. Solís, I. Lobato, E. G. Noya, A. Guerrero-Martínez, J. M. Taboada, F. Obelleiro, L. G. MacDowell, S. Bals and L. M. Liz-Marzán, *Science*, 2020, **368**, 1472–1477.
28 J. Feng, C. Gao and Y. Yin, *Nanoscale*, 2018, **10**, 20492–20504.
29 L. E. González García, N. Ninan, J. Simon, R. Madathiparambil Visalakshan, R. Bright, S. K. Wahono, K. Ostrikov, V. Mailänder, K. Landfester, N. Goswami and K. Vasilev, *Nanoscale*, 2021, **13**, 19936–19945.
30 H. R. Moon, D.-W. Lim and M. P. Suh, *Chem. Soc. Rev.*, 2013, **42**, 1807–1824.
31 W. Yuan and C. M. Li, *Langmuir*, 2009, **25**, 7578–7585.
32 W. Yuan, Z. Lu and C. M. Li, *J. Mater. Chem.*, 2011, **21**, 5148.
33 S. Chakraborty, S. M. Ansar, J. G. Stroud and C. L. Kitchens, *J. Phys. Chem. C*, 2018, **122**, 7749–7758.
34 A. Dhakshinamoorthy and H. Garcia, *Chem. Soc. Rev.*, 2012, **41**, 5262.
35 I. A. Safo, C. Dosche and M. Özaslan, *ChemPhysChem*, 2019, **20**, 3010–3023.
36 I. Krivtsov, D. Mitoraj, C. Adler, M. Ilkaeva, M. Sardo, L. Mafra, C. Neumann, A. Turchanin, C. Li, B. Dietzek, R. Leiter, J. Biskupek, U. Kaiser, C. Im, B. Kirchhoff, T. Jacob and R. Beranek, *Angew. Chem., Int. Ed.*, 2020, **59**, 487–495.
37 A. Savateev and M. Antonietti, *ChemCatChem*, 2019, **11**, 6166–6176.
38 H. Schlomberg, J. Kröger, G. Savasci, M. W. Terban, S. Bette, I. Moudrakovski, V. Duppel, F. Podjaski, R. Siegel, J. Senker, R. E. Dinnebier, C. Ochsenfeld and B. v. Lotsch, *Chem. Mater.*, 2019, **31**, 7478–7486.
39 V. W. Lau, I. Moudrakovski, T. Botari, S. Weinberger, M. B. Mesch, V. Duppel, J. Senker, V. Blum and B. v. Lotsch, *Nat. Commun.*, 2016, **7**, 12165.
40 V. W. Lau and B. v. Lotsch, *Adv. Energy Mater.*, 2022, **12**, 2101078.
41 F. K. Kessler, Y. Zheng, D. Schwarz, C. Merschjann, W. Schnick, X. Wang and M. J. Bojdys, *Nat. Rev. Mater.*, 2017, **2**, 17030.
42 C. Im, B. Kirchhoff, I. Krivtsov, D. Mitoraj, R. Beranek and T. Jacob, *Chem. Mater.*, 2023, **35**, 1547–1559.
43 D. Zheng, J. Zhou, Z. Fang, T. Heil, A. Savateev, Y. Zhang, M. Antonietti, G. Zhang and X. Wang, *J. Mater. Chem. A*, 2021, **9**, 27370–27379.
44 C. Li, E. Hofmeister, I. Krivtsov, D. Mitoraj, C. Adler, R. Beranek and B. Dietzek, *ChemSusChem*, 2021, **14**, 1728–1736.
45 C. Adler, S. Selim, I. Krivtsov, C. Li, D. Mitoraj, B. Dietzek, J. R. Durrant and R. Beranek, *Adv. Funct. Mater.*, 2021, **31**, 2105369.
46 C. Adler, I. Krivtsov, D. Mitoraj, L. Santos-Gómez, S. García-Granda, C. Neumann, J. Kund, C. Kranz, B. Mizaikoff, A. Turchanin and R. Beranek, *ChemSusChem*, 2021, **14**, 2170–2179.
47 I. Krivtsov, A. Vazirani, D. Mitoraj, M. M. Elnagar, C. Neumann, A. Turchanin, Y. Patiño, S. Ordóñez, R. Leiter, M. Lindén, U. Kaiser and R. Beranek, *J. Mater. Chem. A*, 2023, **11**, 2314–2325.
48 J. Strachan, C. Barnett, A. F. Masters and T. Maschmeyer, *ACS Catal.*, 2020, **10**, 5516–5521.
49 D. Patra, S. R. Nalluri, H. R. Tan, M. S. M. Saifullah, R. Ganesan and B. Gopalan, *Nanoscale Adv.*, 2020, **2**, 5384–5395.
50 C. Deraedt, L. Salmon, S. Gatard, R. Ciganda, R. Hernandez, J. Ruiz and D. Astruc, *Chem. Commun.*, 2014, **50**, 14194–14196.
51 B. Saini, L. Khamari and T. K. Mukherjee, *J. Phys. Chem. B*, 2022, **126**, 2130–2141.
52 C. Liang, J. Y. Cheong, G. Sitaru, S. Rosenfeldt, A. S. Schenk, S. Gekle, I. Kim and A. Greiner, *Adv. Mater. Interfaces*, 2022, **9**, 2100867.
53 S. Karimi, A. Moshaii and M. Nikkhah, *Mater. Res. Express*, 2019, **6**, 1150f2.
54 I. Hussain, S. Graham, Z. Wang, B. Tan, D. C. Sherrington, S. P. Rannard, A. I. Cooper and M. Brust, *J. Am. Chem. Soc.*, 2005, **127**, 16398–16399.
55 R. J. Hunter, *Zeta Potential in Colloid Science: Principles and Applications*, Academic Press, 1st edn, 1988.
56 A. Carone, S. Emilsson, P. Mariani, A. Désert and S. Parola, *Nanoscale Adv.*, 2023, **5**, 2017–2026.

57 H. Schlomberg, J. Kröger, G. Savasci, M. W. Terban, S. Bette, I. Moudrakovski, V. Duppel, F. Podjaski, R. Siegel, J. Senker, R. E. Dinnebier, C. Ochsenfeld and B. v. Lotsch, *Chem. Mater.*, 2019, **31**, 7478–7486.
58 X. Hang, S. Wang, H. Pang and Q. Xu, *Chem. Sci.*, 2022, **13**, 461–468.
59 S. K. Ghosh and T. Pal, *Chem. Rev.*, 2007, **107**, 4797–4862.
60 D. Zopes, B. Stein, S. Mathur and C. Graf, *Langmuir*, 2013, **29**, 11217–11226.
61 Y. Wang, J. E. Q. Quinsaat, T. Ono, M. Maeki, M. Tokeshi, T. Isono, K. Tajima, T. Satoh, S. Sato, Y. Miura and T. Yamamoto, *Nat. Commun.*, 2020, **11**, 6089.
62 E. Boisselier and D. Astruc, *Chem. Soc. Rev.*, 2009, **38**, 1759.
63 R. Pamies, J. G. H. Cifre, V. F. Espín, M. Collado-González, F. G. D. Baños and J. G. de la Torre, *J. Nanopart. Res.*, 2014, **16**, 2376.
64 S. Christau, T. Moeller, J. Genzer, R. Koehler and R. von Klitzing, *Macromolecules*, 2017, **50**, 7333–7343.
65 Y. Wang, J. E. Q. Quinsaat, T. Ono, M. Maeki, M. Tokeshi, T. Isono, K. Tajima, T. Satoh, S. Sato, Y. Miura and T. Yamamoto, *Nat. Commun.*, 2020, **11**, 6089.
66 M. Ranka, P. Brown and T. A. Hatton, *ACS Appl. Mater. Interfaces*, 2015, **7**, 19651–19658.
67 L. M. Farigliano, M. A. Villarreal, E. P. M. Leiva and S. A. Paz, *J. Phys. Chem. C*, 2020, **124**, 24009–24016.
68 A. D. McNaught and A. Wilkinson, *Compendium of chemical terminology*, Blackwell Science Oxford, 1997, vol. 1669.
69 A. J. Cohen, P. Mori-Sánchez and W. Yang, *Chem. Rev.*, 2012, **112**, 289–320.
70 R. R. Contreras, P. Fuentealba, M. Galván and P. Pérez, *Chem. Phys. Lett.*, 1999, **304**, 405–413.
71 W. Yang and R. G. Parr, *Proc. Natl. Acad. Sci. U. S. A.*, 1985, **82**, 6723–6726.
72 P. J. Flory, *Principles of polymer chemistry*, Cornell University Press, 1953.
73 A. Stukowski, *Modell. Simul. Mater. Sci. Eng.*, 2010, **18**, 015012.
74 J. Zeng, Q. Zhang, J. Chen and Y. Xia, *Nano Lett.*, 2010, **10**, 30–35.
75 S. Wunder, Y. Lu, M. Albrecht and M. Ballauff, *ACS Catal.*, 2011, **1**, 908–916.
76 Z. Zhang and Y. Wu, *Langmuir*, 2010, **26**, 9214–9223.